
Impacts of Space Shuttle Thermal Protection System Tile on an F-15 Aircraft Vertical Tail

William L. Ko

March 1985

Impacts of Space Shuttle Thermal Protection System Tile on an F-15 Aircraft Vertical Tail

William L. Ko

Ames Research Center, Dryden Flight Research Facility, Edwards, California

1985



National Aeronautics and
Space Administration

Ames Research Center

Dryden Flight Research Facility
Edwards, California 93523

SUMMARY

Impacts of the space shuttle thermal protection system (TPS) tile on the leading edge and the side of the vertical tail of the F-15 aircraft were analyzed under different TPS tile orientations. The TPS tile-breaking tests were conducted to simulate the TPS tile impacts. It was found that the predicted tile impact forces compared fairly well with the results of the tile-breaking tests, and the impact forces exerted on the F-15 aircraft vertical tail were relatively low because a very small fraction of the tile kinetic energy was dissipated in the impact, penetration, and fracture of the tile. It was also found that the oblique impact of the tile on the side of the F-15 aircraft vertical tail was unlikely to dent the tail surface.

INTRODUCTION

The space shuttle orbiter reenters the earth's atmosphere at an altitude of 121.92 km (400,000 ft) and at an extremely high velocity (nearly Mach 25 at the beginning of reentry). Because of severe reentry aerodynamic heatings, the entire shuttle structure is protected with a thermal protection system (TPS). There are three types of TPS: (1) felt reusable surface insulation (FRSI), (2) low temperature reusable surface insulation (LRSI), and (3) high temperature reusable surface insulation (HRSI). The FRSI is a highly flexible blanket-type layer of heat shield that is bonded to the low heating zones of the shuttle (for example, upper wing and the cargo bay door surfaces) using room temperature vulcanized (RTV) rubber. The LRSI and HRSI (both are called TPS tiles) are low-density porous silica tiles with an average size of 15.20 m (6 in) square, each individually bonded (using RTV) to the shuttle structure through a layer of strain isolation pad (SIP). The SIP layer is highly flexible and serves as a cushion to absorb thermal strain incompatibility between the TPS tiles and the aluminum structure. The LRSI is used in medium heating areas such as the upper glove and the upper wing surface near the leading edge. The HRSI is used in the highly heated areas, such as the lower wing and the fuselage bottom surfaces. Some of the gaps between the TPS tiles in the high temperature areas are filled with ceramic coated alumina mat (gap fillers) to prevent hot gases from coming in contact with the substructure at the bottom of each gap.

Before the space transportation system, trajectory 1 (STS-1) flight, the shuttle orbiter, Columbia, was transported on top of a Boeing-747 aircraft from California to Kennedy Space Center in Florida. During the ferry flight, some of the TPS tiles and gap fillers in areas subjected to high air loads loosened or migrated. This unexpected occurrence, even at modest flight conditions and air loads, raised questions about the structural integrity of the TPS tiles and gap filler system during the actual STS flight (lift-off and reentry) and initiated a series of tests on the effects of high air loads on the TPS tiles and gap filler system. The tests were done by bonding the TPS tiles near the leading-edge region of the F-15 aircraft wing. Air loads on the tiles were generated by flying the F-15 aircraft under certain flight envelopes to simulate the air loads on the concerned regions of the shuttle. One of the main concerns in this simulated air loads test was the impact of the TPS tiles on the F-15 aircraft tail if the TPS tiles should separate from the F-15 aircraft wing during the test flights. To estimate the impact force of the TPS tile on the F-15 aircraft vertical tail and to examine the degree of damage the TPS tile would produce on the F-15 tail, impact analysis was performed and compared with

laboratory TPS tile-breaking tests. This report presents the results of the analysis of the impact of TPS tile on the F-15 aircraft vertical tail and the simulated impact, penetration, and fracture tests of the TPS tiles.

NOMENCLATURE

A	area, surface area of TPS
a	length of TPS
b	width of TPS
c	thickness of TPS
E	kinetic energy, J (in-lb), or modulus of elasticity, N/m^2 (lb/in ²)
F	force, N (lb)
FRSI	felt reusable surface insulation
g	gravitational acceleration, m/sec^2 (ft/sec ²)
HRSI	high temperature reusable surface insulation
I	moment of inertia, m^4 (in ⁴)
LRSI	low temperature reusable surface insulation
l	depth of the honeycomb core of the vertical tail
M	moment, N-m (in-lb)
P	force exerted on tail side surface by TPS, N (lb)
q	dynamic pressure, N/m^2 (lb/ft ²)
RTV	room temperature vulcanized
s	distance, m (ft)
SIP	strain isolation pad
STS	space transportation system
TPS	thermal protection system
t	time, sec
U	energy used in breaking TPS, J (in-lb)

V	velocity, m/sec (in/sec)
W	weight, N (lb)
x,y	Cartesian coordinates
α	acceleration, m/sec ² (in/sec ²)
ϵ	strain, m/m (in/in)
θ	oblique impact angle, deg
ξ	dummy coordinate in x-direction
ρ	density, kg/m ³ (lb/ft ³)
σ_b	bending stress, N/m ² (lb/in ²)
σ_c	TPS compressive strength (crushing strength), N/m ² (lb/in ²)
σ_T	TPS tensile strength, N/m ² (lb/in ²)
σ_t	tensile stress, N/m ² (lb/in ²)
τ	TPS shearing strength, N/m ² (lb/in ²)

Superscripts:

N	component normal to the tail surface
---	--------------------------------------

Subscripts:

al	quantities associated with aluminum material
cr	crushing
eff	effective quantities
hc	quantities associated with honeycomb core of the tail
m	maximum penetration distance
tail	quantities associated with the tail
1	mode 1
2	mode 2
3	mode 3

DESCRIPTION OF PROBLEM

Figure 1 is an illustration of the F-15 aircraft with the TPS test article installed near the leading edge of the wing for the air load tests. The F-15 aircraft was chosen because of its ability to match the shuttle orbiter flow fields and its large Mach number and dynamic pressure envelope (ref. 1). Through a specific maneuver of the F-15 aircraft, the desired dynamic pressure acting on the concerned region of the shuttle orbiter could be simulated on the surface of the TPS test article. During the test flights, if one of the TPS tiles should separate from the TPS test article, it could impact on either the leading edge or the side of the F-15 aircraft vertical tail. A study was undertaken to estimate the impact loads of the TPS tile on the F-15 aircraft vertical tail under different tile orientations and to determine the degree of seriousness of the impacts. F-15 aircraft and the TPS data used in this report are listed below.

TPS tile - F-15 tail distance (s), m (in)	5.79 (228)
Dynamic pressure (q), N/m ² (lb/ft ²)	52,668 (1100)
TPS tile weight (W), each, N (lb)	2.22 (0.5)
TPS tile density (ρ), kg/m ³ (lb/ft ³)	144.17 (9)
TPS tile tensile strength (σ _T), N/m ² (lb/in ²)	1.4479 × 10 ⁵ (21)
TPS tile compressive strength (crushing strength, σ _C), N/m ² (lb/in ²)	4.8263 × 10 ⁵ (70)
TPS tile shearing strength (τ), N/m ² (lb/in ²)	1.5860 × 10 ⁵ (23)
TPS tile dimensions, width (a), length (b), thickness (c), cm (in)	a = b = 15.24 (6.0)
.....	c = 6.35 to 6.99 (2.50 to 2.75)
Gravitational acceleration (g), m/sec ² (ft/sec ²)	9.81 (32.2)

IMPACT VELOCITIES OF TPS TILES

If one TPS tile should separate from the test article, under the dynamic pressure (q) during the test flight, the tiles will travel at different velocities toward the F-15 aircraft tail, depending on their orientation. Figure 2 shows the three tile orientations considered.

Mode 1 Impact

Consider the TPS tile is oriented in such a way that the plane A₁ (area = a × b) is normal to the air flow (with dynamic pressure, q, see top of fig. 2). From Newton's second law, the acceleration α₁ of the TPS at the time of debonding may be calculated from

$$A_1 q = \frac{W}{g} \alpha_1 \quad (1)$$

which gives, after substitution of the given data,

$$\alpha_1 = 2.6962 \times 10^2 \text{ m/sec}^2 \text{ (1.0615} \times 10^5 \text{ in/sec}^2) \quad (2)$$

The time t_1 required for the TPS to travel a distance s (time lag between the TPS debonding and its impact on the F-15 aircraft tail) can be obtained from

$$s = \frac{1}{2} \alpha_1 t_1^2 \quad (3)$$

which gives

$$t_1 = 6.5542 \times 10^{-2} \text{ sec} \quad (4)$$

after substitution of the numerical values.

The velocity V_1 of the TPS at the time of impact on the F-15 aircraft tail can be obtained from

$$V_1 = \alpha_1 t_1 \quad (5)$$

or

$$V_1 = 176.72 \text{ m/sec} = 6.9573 \times 10^3 \text{ in/sec} = 395 \text{ mi/hr} \quad (6)$$

The kinetic energy E_1 of the TPS at the time of impact is calculated from

$$E_1 = \frac{1}{2} \frac{W}{g} V_1^2 \quad (7)$$

which gives

$$E_1 = 3542 \text{ J (3.1350} \times 10^4 \text{ in-lb)} \quad (8)$$

Mode 2 Impact

If the TPS is oriented with area A_2 ($= a \times c$) normal to the vector q (see middle of fig. 2), the acceleration α_2 of the TPS at the time of debonding will be

$$\alpha_2 = \frac{g}{W} A_2 q = 2.2515 \times 10^3 \text{ m/sec}^2 \text{ (0.8864} \times 10^5 \text{ in/sec}^2) \quad (9)$$

and the time t_2 for the TPS to travel a distance s will be

$$t_2 = \sqrt{\frac{2s}{\alpha_2}} = 7.1797 \times 10^{-2} \text{ sec} \quad (10)$$

The velocity V_2 of the TPS at the time of impact is

$$V_2 = \alpha_2 t_2 = 161.32 \text{ m/sec} = (6.3512 \times 10^3 \text{ in/sec} = 361 \text{ mi/hr}) \quad (11)$$

The kinetic energy E_2 of the TPS at the instant of impact will be

$$E_2 = \frac{1}{2} \frac{W}{g} V_2^2 \quad (12)$$

or

$$E_2 = 2952 \text{ J } (2.6125 \times 10^4 \text{ in-lb}) \quad (13)$$

which is lower than E_1 as expected because $A_2 < A_1$.

Mode 3 Impact

For the TPS orientation with area A_3 ($= A_2$) facing vector q (shown in the bottom of fig. 3), the acceleration α_3 , the t_3 for the TPS to travel a distance s , the TPS velocity V_3 at the time of impact, and the TPS kinetic energy E_3 at the time of impact are identical to those for the mode 2 impact. That is,

$$\alpha_3 = \alpha_2 = 2.2515 \times 10^3 \text{ m/sec}^2 \text{ } (0.8846 \times 10^5 \text{ in/sec}^2) \quad (14)$$

$$t_3 = t_2 = 7.1797 \times 10^{-2} \text{ sec} \quad (15)$$

$$V_3 = V_2 = 161.32 \text{ m/sec} = 6.3512 \times 10^3 \text{ in/sec} = 361 \text{ mi/hr} \quad (16)$$

$$E_3 = E_2 = 2952 \text{ J } (2.6125 \times 10^4 \text{ in-lb}) \quad (17)$$

F-15 AIRCRAFT VERTICAL TAIL

Figure 3 shows the geometry of the leading-edge region of the F-15 aircraft vertical tail. The tail profile may be expressed with the following parabolic equation

$$y = K \sqrt{x} \quad (18)$$

where K is a constant and was determined by curve fitting to be

$$K = 0.99 \sqrt{\text{cm}} \text{ } (0.62 \sqrt{\text{in}}) \quad (19)$$

IMPACTS OF TPS ON AIRCRAFT TAIL LEADING EDGE

The TPS is a porous material and contains approximately 90-percent voids. It is very brittle and is easily crushed. Thus the impact of the TPS tile on the F-15 aircraft tail may be considered a crushing, and not an elastic, impact. During the crushing impact, the leading-edge region of the tail will first penetrate into the TPS tile and will then break up the tile. This implies that only a small amount of the TPS kinetic energy will be used in loading the tail. Impact analysis will be performed for three orientations of the TPS tile as shown in figure 4. It is

assumed that the mode 1 impact will induce the bending fracture and both the mode 2 and mode 3 impacts will result in wedge fractures.

Mode 1 Impact

When the TPS tile is oriented as shown in figures 4 and 5, the mode 1 fracture (bending fracture) is likely to take place. During the crushing (or penetration) period, the force $F_1(x)$ exerted on the TPS tile by the tail (or the force exerted on the tail by the TPS tile) will be

$$F_1(x) = 2yb\sigma_c + 2xb\tau \quad (20)$$

where

$2yb\sigma_c$ = compressive crushing term

$2xb\tau$ = shear crushing term

Substitution of equation (18) into equation (20) yields

$$F_1(x) = 2b(\sigma_c K \sqrt{x} + \tau x) \quad (21)$$

When the penetration depth x reaches a certain critical value $x = x_m$, the TPS tile breaks into two pieces because of the bending moment induced by $\frac{F_1}{2}$ acting on the upper and lower halves of the tile. The critical penetration depth x_m may be calculated as follows.

From Timoshenko's Theory of Elasticity (ref. 2), the tensile stress σ_t at the outermost fiber of a deep beam (consider TPS tile as a deep beam) may be expressed as (see fig. 5)

$$b\sigma_t = \frac{3F_1(x)}{2h^3} \left(\frac{d}{2} - \frac{h}{\pi} \right) h + \frac{F_1(x)}{2\pi h} \quad (22)$$

where $h = c/2$, $d = a/4$.

When σ_t reaches its critical value σ_T (or x reaches x_m), equation (22) becomes

$$\sigma_T = \frac{F_1 x_m}{2bh} \left(\frac{3}{2} \frac{d}{h} - \frac{2}{\pi} \right) \quad (23)$$

Combining equations (20) and (23) for $x = x_m$, there results

$$x_m = \frac{1}{2} \left(\frac{\sigma_c}{\tau} \right)^2 \left[\left(2B \frac{\tau}{\sigma_c} + K^2 \right) \pm K \sqrt{4B \frac{\tau}{\sigma_c} + K^2} \right] \quad (24)$$

where

$$B = \frac{\sigma_{Th}}{\sigma_c \left(\frac{3}{2} \frac{d}{h} - \frac{2}{\pi} \right)} \quad (25)$$

Applying the given numerical values, equation (24) yields the maximum penetration depth x_m as

$$x_m = 0.56 \text{ cm (0.22 in)} \quad (26)$$

which is quite shallow.

From equations (21) and (26), and using the given data, the maximum crushing force $F_1(x_m)$ is determined as

$$F(x_m) = 1366 \text{ N (307 lb)} \quad (27)$$

The energy U_1 dissipated in penetration and breaking the tile can be calculated from

$$U_1 = \int_0^{x_m} F(x) dx = 2b \int_0^{x_m} (\sigma_c K \sqrt{x} + \tau x) dx \quad (28)$$

which, after integration, gives

$$U_1 = bx_m \left(\frac{4}{3} \sigma_c K \sqrt{x_m} + \tau x_m \right) \quad (29)$$

Applying the numerical values, there results

$$U_1 = 4.84 \text{ J (42.85 in-lb)} \quad (30)$$

which is only 0.13 percent of the original kinetic energy of the TPS tile E_1 (see eq. (8)) at mode 1 orientation. The remaining kinetic energy of the tile can never be used in loading the tail, and is carried away by the broken pieces of the tile.

The velocity of the tile, V_1' , after the impact will be

$$V' = \sqrt{\frac{2g}{W}(E_1 - U_1)} = 176.69 \text{ m/sec} = (6.9562 \times 10^3 \text{ in/sec}) \quad (31)$$

Comparing equations (6) and (31), the velocity loss of the tile will be

$$V_1 - V_1' = 0.028 \text{ m/sec (1.1 in/sec)} \quad (32)$$

which is extremely small compared with V_1 , and thus the impact hardly affects the velocity of the tile.

Mode 2 Impact

During the mode 2 impact, penetration, and fracture, the wedge effect of the tail leading-edge region will induce a tensile stress field in the tile along the x-axis ahead of the tail (see fig. 6). At the same time, the bending moment

$$M = \frac{1}{2} F_2(x)d \quad (33)$$

will induce compressive stress σ_b at the tip of the notch. Thus for the tile to fail in tension, the tensile stress induced by the tail wedge action at the tip of the notch has to reach $(\sigma_t + \sigma_b) = \sigma_T + \sigma_b \big|_{x=x_m}$ at the time of tensile failure. The crushing force $F_2(x)$ can be written as

$$F_2(x) = 2c(\sigma_c K \sqrt{x} + \tau x) \quad (34)$$

where

$2c\sigma_c K \sqrt{x}$ = compressive crushing term

$2c\tau x$ = shear crushing term

The bending stress σ_b can be calculated from

$$\sigma_b = \frac{M}{I} \left(\frac{b-x}{2} \right) \quad (35)$$

where

$$I = \frac{1}{12} c(b-x)^3 \quad (36)$$

Combining equations (33) to (36), σ_b can be expressed as

$$\sigma_b = \frac{6d(\sigma_c K \sqrt{x} + \tau x)}{(b-x)^2} \quad (37)$$

Assuming the stress distribution in the tile along the x-axis ahead of the tail leading edge to be parabolic and given by

$$\sigma(\xi) = \frac{\sigma_t + \sigma_b}{(b-x)^2} \xi^2 \quad (38)$$

The integration of $\sigma(\xi)$ from $\xi = 0$ to $\xi = b - x$ must be balanced by the wedge force $\sigma_c x$. Thus

$$\sigma_c x = \int_0^{b-x} \sigma(\xi) d\xi \quad (39)$$

With equations (37) and (38) considered, equation (39) can be integrated to yield

$$\left(\sigma_c + \frac{\sigma_t}{3}\right)x = \frac{\sigma_t b}{3} + \frac{2d(\sigma_c K \sqrt{x} + \tau x)}{b - x} \quad (40)$$

The maximum penetration depth $x = x_m$ at the time of fracture can be calculated from equation (40) by setting $\sigma_t = \sigma_T$ and $x = x_m$. Applying the known numerical values, x_m is determined to be

$$x_m = 2.84 \text{ cm (1.12 in)} \quad (41)$$

From equations (34) and (41), the maximum crushing load at the time of the tile fracture can be calculated as

$$F_2(x_m) = 1677 \text{ N (377 lb)} \quad (42)$$

The energy U_2 used in breaking the tile is

$$U_2 = \int_0^{x_m} F_2(x) dx = 2c \int_0^{x_m} (\sigma_c K \sqrt{x} + \tau x) dx \quad (43)$$

which, after integration, gives

$$U_2 = cx_m \left(\frac{4}{3} \sigma_c K \sqrt{x_m} + \tau x_m \right) \quad (44)$$

Applying the known numerical values, it is found that

$$U_2 = 28.95 \text{ J (256.27 in-lb)} \quad (45)$$

which is only 0.98 percent of the original kinetic energy E_2 of the tile (see eq. (17)) at mode 2 orientation. The velocity of the tile, V_2' , after the impact fracture is

$$V_2' = \sqrt{\frac{2g}{W}(E_2 - U_2)} = 160.61 \text{ m/sec (6.3232} \times 10^3 \text{ in/sec)} \quad (46)$$

The tile velocity loss will then be

$$V_2 - V_2' = 0.71 \text{ m/sec (28 in/sec)} \quad (47)$$

which is just 0.44 percent of the original tile velocity before impact.

Mode 3 Impact

For mode 3 impact, penetration, and fracture (see fig. 7), the bending effect caused by bending moment $M = \frac{1}{2} cF_3(x)$ may be neglected. The crushing load $F_3(x)$ for this case is given by

$$F_3(x) = 2a(\sigma_c K \sqrt{x} + \tau x) \quad (48)$$

where

$2a\sigma_c K \sqrt{x}$ = compressive crushing term

$2a\tau x$ = shear crushing term

Assuming that the penetrating leading-edge portion of the tail induces a parabolic stress distribution along the x-axis ahead of the leading edge then

$$\sigma(\xi) = \frac{\sigma_t}{(b-x)^2} \xi^2 \quad (49)$$

From the force balance (that is, notch opening force = tile resisting force) there results

$$\sigma_c x = \int_0^{b-x} \sigma(\xi) d\xi \quad (50)$$

which, with equation (49) substituted and integrated, becomes

$$x = \frac{\sigma_t b}{3\sigma_c + \sigma_t} \quad (51)$$

The maximum penetration depth $x = x_m$ occurs when σ_t reaches the tensile strength σ_T of the tile; that is,

$$x_m = \frac{\sigma_T b}{3\sigma_c + \sigma_T} \quad (52)$$

Applying the known numerical values into equation (52), x_m is found to be

$$x_m = 1.40 \text{ cm (0.55 in)} \quad (53)$$

The maximum crushing load $F_3(x_m)$ at the instant of tile fracture is then obtained from equation (48) by setting $x = x_m$

$$F_3(x_m) = 2393 \text{ N (538 lb)} \quad (54)$$

The energy dissipated in fracturing the tile is

$$U_3 = \int_0^{x_m} F_3(x) dx = 2a \int_0^{x_m} (\sigma_c K \sqrt{x} + \tau x) dx \quad (55)$$

which, after integration, becomes

$$U_3 = ax_m \left(\frac{4}{3} \sigma_c K \sqrt{x_m} + \tau x_m \right) \quad (56)$$

Applying the given numerical values to equation (56), the value of U_3 is found to be

$$U_3 = 20.72 \text{ J (183.37 in-lb)} \quad (57)$$

which is only 0.7 percent of the tile kinetic energy E_3 before impact.

The velocity of the tile V_3' after impact can be obtained from

$$V_3' = \sqrt{\frac{2g}{W}(E_3 - U_3)} = 160.84 \text{ m/sec (6.3321} \times 10^3 \text{ in/sec)} \quad (58)$$

The tile velocity loss will then be

$$V_3 - V_3' = 0.48 \text{ m/sec (19.1 in/sec)}$$

which is only 0.3 percent of the original tile velocity V_3 before impact.

OBLIQUE IMPACTS OF TPS ON TAIL SIDE SURFACE

The oblique impacts of the TPS tile on the side surface of the F-15 aircraft tail can happen when the aircraft is making a turn or is side slipping. When the TPS tile impacts on the tail side surface, the component of the tile kinetic energy normal to the tail surface could be dissipated in compacting (or crushing from porous state into solid state) the tile, and deforming the tail surface sheet and the honeycomb core. Figure 8 shows the three modes of oblique impacts. If the TPS tile strikes on the tail surface at an angle θ , the kinetic energy E_i^N ($i = 1, 2, 3$) associated with the velocity component V_i^N ($i = 1, 2, 3$) normal to the tail surface will be

Mode 1

$$E_1^N = E_1 \tan^2 \theta \quad (59)$$

Mode 2

$$E_2^N = E_2 \tan^2 \theta \quad (60)$$

Mode 3

$$E_3^N = E_3 \tan^2 \theta \quad (61)$$

If $\theta = 20^\circ$, the numerical values of E_i^N ($i = 1, 2, 3$) can be calculated using equations (8), (13), and (17)

Mode 1

$$E_1^N = 469.24 \text{ J } (4.1531 \times 10^3 \text{ in-lb}) \quad (62)$$

Mode 2

$$E_2^N = 391.03 \text{ J } (3.4609 \times 10^3 \text{ in-lb}) \quad (63)$$

Mode 3

$$E_3^N = 391.03 \text{ J } (3.4609 \times 10^3 \text{ in-lb}) \quad (64)$$

For the tile with 90 percent void content, the crushing energy E_{cr} (energy required to compact the tile into solid) for all three tail orientations may be written as

$$E_{cr} = 0.9abc\sigma_c \quad (65)$$

which gives

$$E_{cr} = 640.62 \text{ J } (5.67 \times 10^3 \text{ in-lb}) \quad (66)$$

It is seen that the tile crushing energy E_{cr} is larger than E_i^N for the three modes of oblique impacts. This implies that all of the normal kinetic energy E_i^N will be dissipated in partially compacting the tile (see fig. 9). Thus the pressure σ_{tail} exerted on the tail surface by the tile will be

$$\sigma_{tail} = \sigma_c = 4.8263 \times 10^5 \text{ N/m}^2 \text{ (70 lb/in}^2\text{)} \quad (67)$$

which is the compressive crushing stress of the TPS tile.

DEFORMATION OF TAIL

The interior of the F-15 aircraft vertical tail is made of aluminum honeycomb core. A typical honeycomb core used in high-speed aircraft has the effective modulus of elasticity E_{eff} in the honeycomb core thickness direction of the order of

$$\frac{E_{eff}}{E_{al}} = 2.1 \times 10^{-2} \quad (68)$$

where $E_{al} = 6.8948 \times 10^{10} \text{ N/m}^2$ (10^7 lb/in^2) is the modulus of elasticity for aluminum material. With the numerical value of E_{al} applied, equation (68) becomes

$$E_{eff} = 1.4479 \times 10^9 \text{ N/m}^2 \text{ (} 2.1 \times 10^5 \text{ lb/in}^2 \text{)} \quad (69)$$

The strain ϵ of the honeycomb core in the tail thickness direction (see fig. 9) can be written as (neglecting the face sheet bending effect)

$$\epsilon = \frac{\sigma_{tail}}{E_{eff}} \quad (70)$$

With numerical values applied, ϵ becomes

$$\epsilon = 3.3333 \times 10^{-4} \text{ m/m (in/in)} \quad (71)$$

The stress σ_{hc} induced in the honeycomb core by the strain ϵ is then

$$\sigma_{hc} = \epsilon E_{al} \quad (72)$$

or

$$\sigma_{hc} = 2.2980 \times 10^7 \text{ N/m}^2 \text{ (} 3.333 \times 10^3 \text{ lb/in}^2 \text{)} \quad (73)$$

The yield stresses for most of the aluminum materials are in the range of $9.6527 \times 10^7 \text{ N/m}^2$ ($14 \times 10^3 \text{ lb/in}^2$) to $25.5106 \times 10^7 \text{ N/m}^2$ ($37 \times 10^3 \text{ lb/in}^2$). Thus σ_{hc} is well below the yield stress and therefore, the possibility of denting the tail surface because of oblique impacts of the tile is remote.

The forces P_i ($i = 1, 2, 3$) exerted on the tail surface because of the three modes of oblique impacts are given by

Mode 1

$$P_1 = bc\sigma_c = 4671 \text{ N (} 1.05 \times 10^3 \text{ lb)} \quad (74)$$

Mode 2

$$P_2 = bc\sigma_c = 4671 \text{ N (} 1.05 \times 10^3 \text{ lb)} \quad (75)$$

Mode 3

$$P_3 = ab\sigma_c = 11210 \text{ N (} 2.52 \times 10^3 \text{ lb)} \quad (76)$$

TPS TILE-BREAKING TESTS

To measure the TPS tile impact forces (F_1 , F_2 , F_3) on the F-15 aircraft vertical tail, several quasistatic tile-breaking tests were conducted. Figure 10 shows three modes of loading in the tile-breaking tests. For the loading of modes 1 and 2, the tile was supported by two foam rubber bars to induce bending moment for simulating the bending caused by the tile inertia forces acting on both sides of the tail leading edge (see figs. 5 and 6). For mode 3 loading, no foam rubber was used. For mode 1 loading only, a thick layer of foam rubber support was also used for simulating the uniform aerodynamic pressure (see fig. 11). The setup for the tile-breaking test is shown in figure 11. The F-15 aircraft tail fixture simulation was made of a thick aluminum plate formed into the contour of the leading-edge region of the F-15 aircraft vertical tail.

RESULTS

Figures 12, 13, and 14 show the fractured TPS tiles after the modes 1, 2, and 3 tile-breaking tests, respectively. The results of the tile-breaking tests are summarized in table 1. It can be seen that for the modes 2 and 3 impacts, the predicted tile impact forces F_2 and F_3 compare fairly well with their associated tile-breaking forces. For the mode 1 impact, the predicted tile impact force F_1 appears to be slightly lower than the averaged value of the tile-breaking forces. The first three values of the data for F_1 were obtained from the case when the tiles were supported by two foam rubber bars (see fig. 10), and the last two values, which are higher, were obtained from the case when the tile was supported by a thick layer of foam rubber. If the last two data are neglected, the predicted value of F_1 compares reasonably well with the averaged values of the first three tile-breaking forces.

CONCLUSIONS

Analyses were performed on the impacts of the space shuttle TPS tile on the leading edge and the side of the F-15 aircraft vertical tail under different tile orientations. In addition, tile-breaking tests were conducted to simulate the tile impacts. From the tile impact analyses and the tile-breaking tests, the following conclusions can be drawn.

1. Because of low tensile strength, the TPS tile breaks immediately after impact, and a very small fraction of the TPS kinetic energy is dissipated in the impact, penetration, and fracture of the tile. Thus the impact force exerted by the tile on the leading edge of the F-15 aircraft vertical tail is relatively low. After the impact the broken tile pieces continue to travel at a velocity very close to the original tile velocity before the impact.

2. In the 20° oblique impact, all the tile kinetic energy component normal to the F-15 aircraft vertical tail side surface is consumed in partial compacting of the tile.

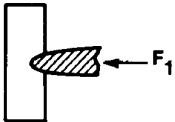
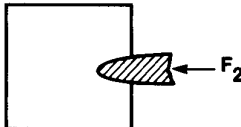

3. The strain induced in the honeycomb core of the F-15 aircraft vertical tail caused by the 20° oblique tile impact on the side of the tail was found to be well below the yielding strain and, therefore, the possibility of denting the tail surface is remote.

4. The predicted tile-impact forces in three tile orientations compare fairly well with the experimental tile-breaking forces. This indicates that the tile-impact analysis was quite adequate.

REFERENCES

1. Meyer, Robert R., Jr.; Jarvis, Calvin R.; and Barneburg, Jack: In-Flight Aerodynamic Testing of the Shuttle Thermal Protection System. AIAA Paper No. 81-2468, Nov. 1981.
2. Timoshenko, S. P.; and Goodier, J. N.: Theory of Elasticity, 3rd Ed., McGraw-Hill Book Co., Inc., 1970.
3. Ko, William L.: Comparison of Structural Behavior of Superplastically Formed/Diffusion-Bonded Sandwich Structures and Honeycomb Core Sandwich Structures. NASA TM-81343, 1980.
4. Ko, William L.: Elastic Constants for Superplastically Formed/Diffusion-Bonded Corrugated Sandwich Core. NASA TP-1562, 1980.

TABLE 1. - TPS IMPACT FORCES

Mode	Predicted tile impact forces	Measured tile-breaking forces
Mode 1 	$F_1 = 1366 \text{ N}$ (307 lb)	$F_1 = \begin{cases} 1557 \text{ N (350 lb)} \\ 1032 \text{ N (232 lb)} \\ 1721 \text{ N (387 lb)} \\ 2157 \text{ N (530 lb)} \\ 2358 \text{ N (485 lb)} \end{cases}$ Average 1765 N (397 lb)
Mode 2 	$F_2 = 1592 \text{ N}$ (358 lb)	$F_2 = \begin{cases} 1570 \text{ N (353 lb)} \\ 2028 \text{ N (456 lb)} \\ 1690 \text{ N (380 lb)} \end{cases}$ Average 1763 N (396 lb)
Mode 3 	$F_3 = 2393 \text{ N}$ (538 lb)	$F_3 = \begin{cases} 2055 \text{ N (462 lb)} \\ 2682 \text{ N (603 lb)} \\ 2393 \text{ N (538 lb)} \end{cases}$ Average 2377 N (534 lb)

*TPS tile was supported by a layer of foam rubber.

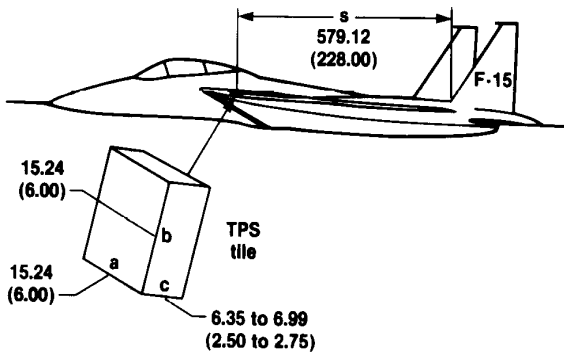


Figure 1. The F-15 aircraft with TPS attached to the leading edge of its wing. Dimensions are in centimeters (inches).

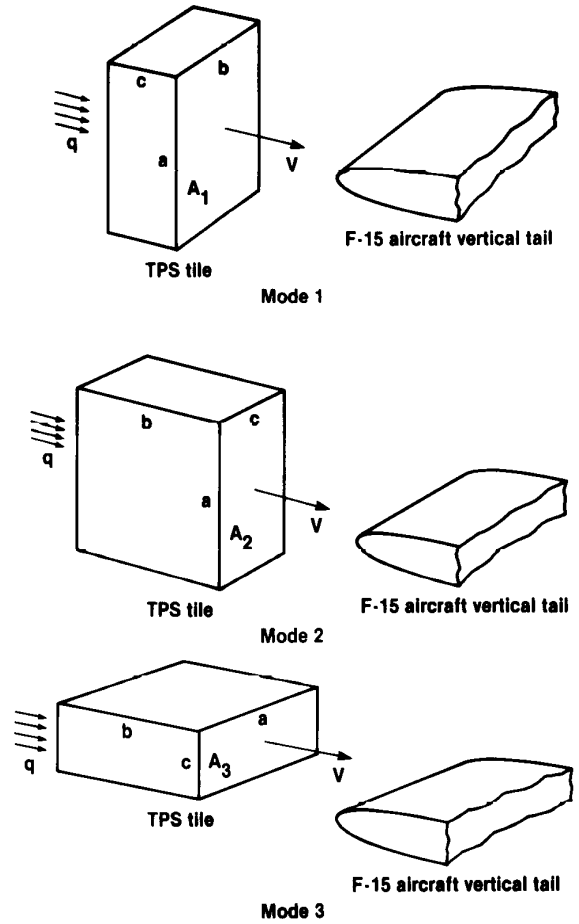


Figure 2. Configurations of impacts of TPS tile on F-15 aircraft vertical tail.

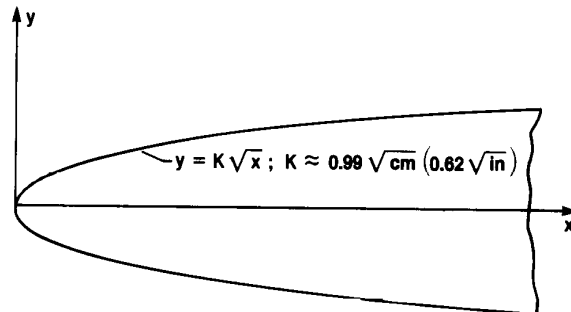


Figure 3. Geometry of the F-15 aircraft vertical tail leading-edge cross section.

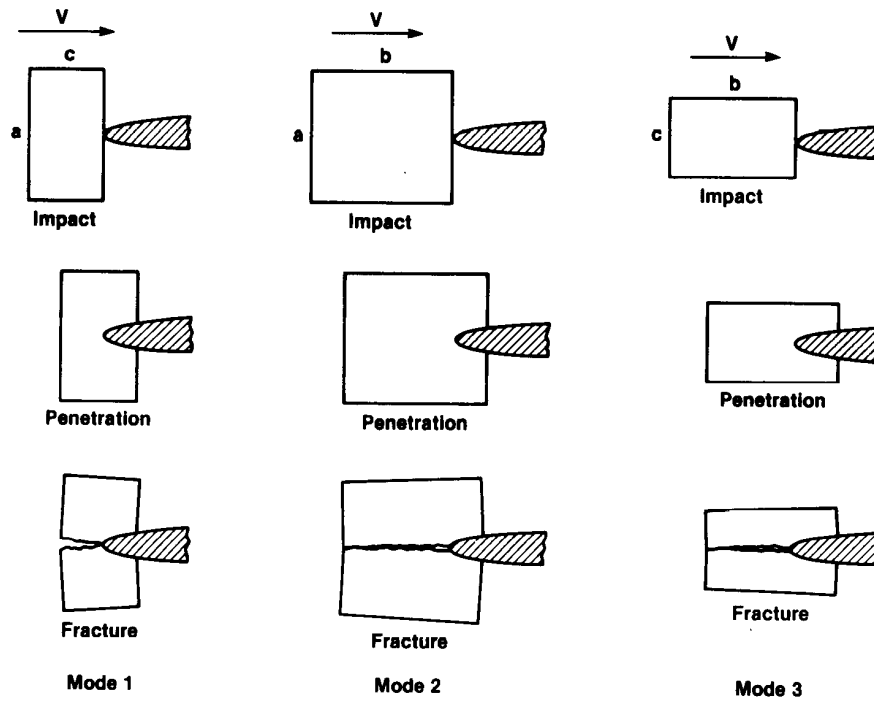


Figure 4. Three modes of impact, penetration, and fracture.

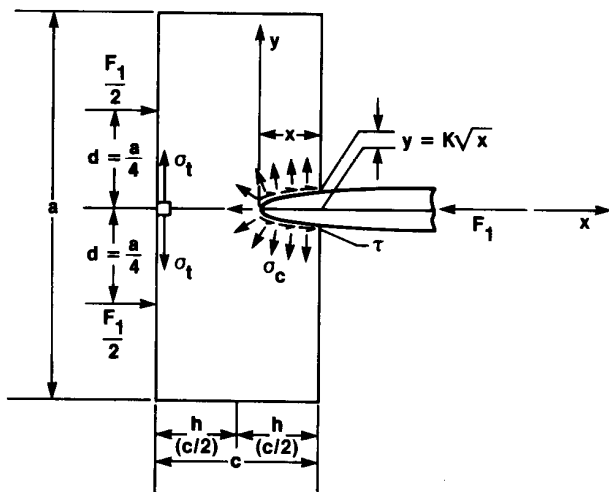


Figure 5. Mode 1 impact.

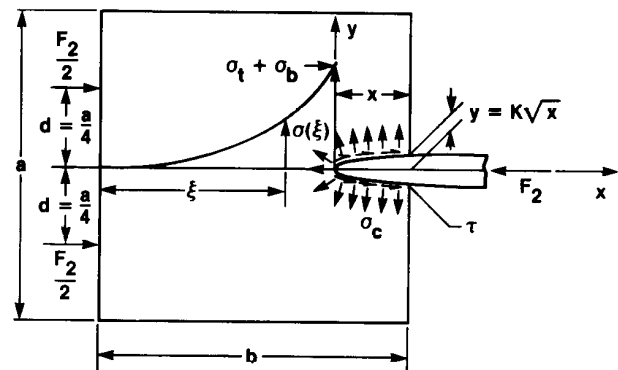
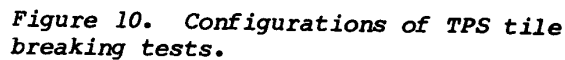
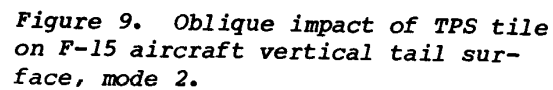
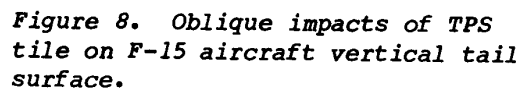
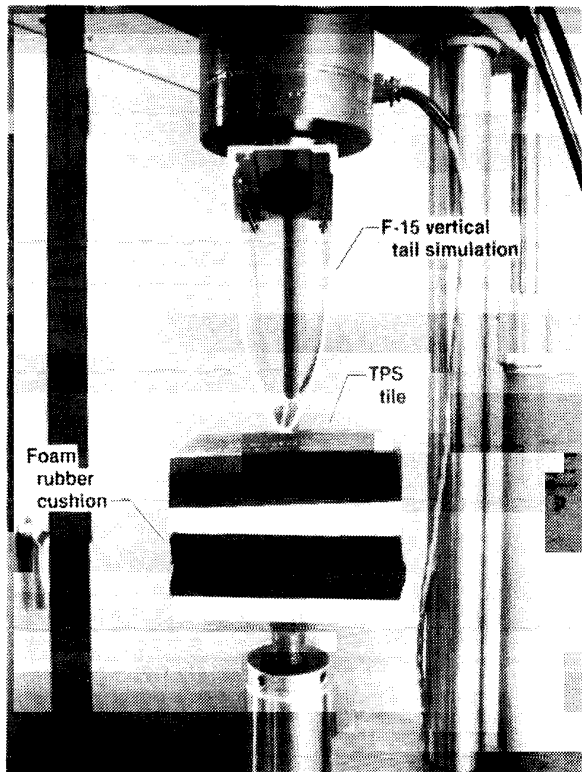


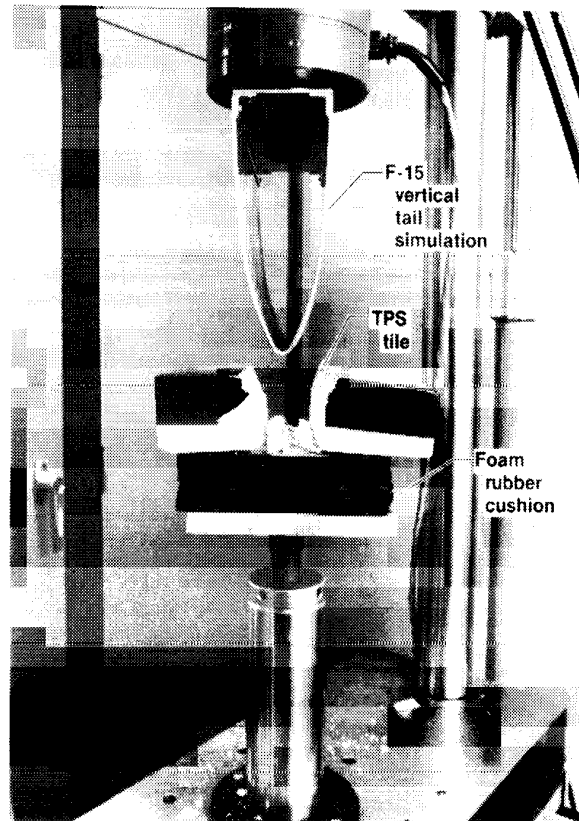
Figure 6. Mode 2 impact.





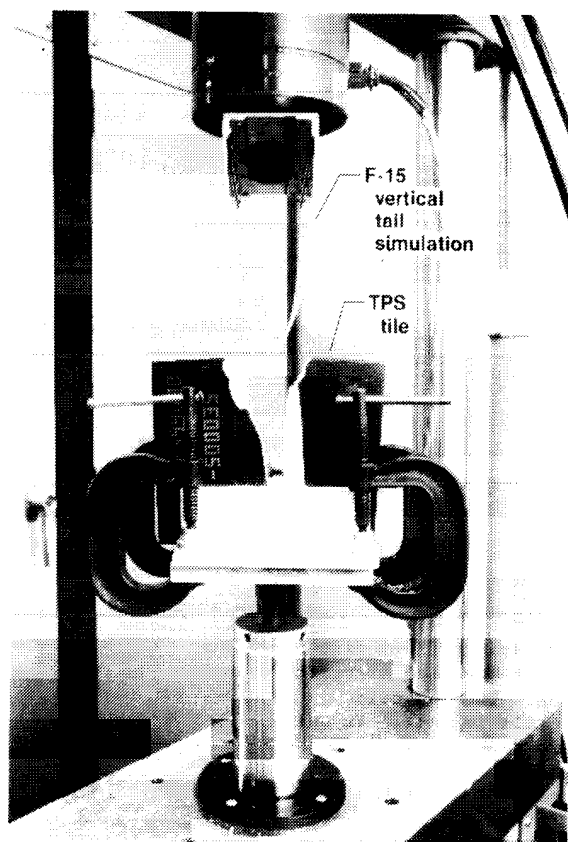
ECN 11324

Figure 11. Experimental setup for TPS tile-breaking test.



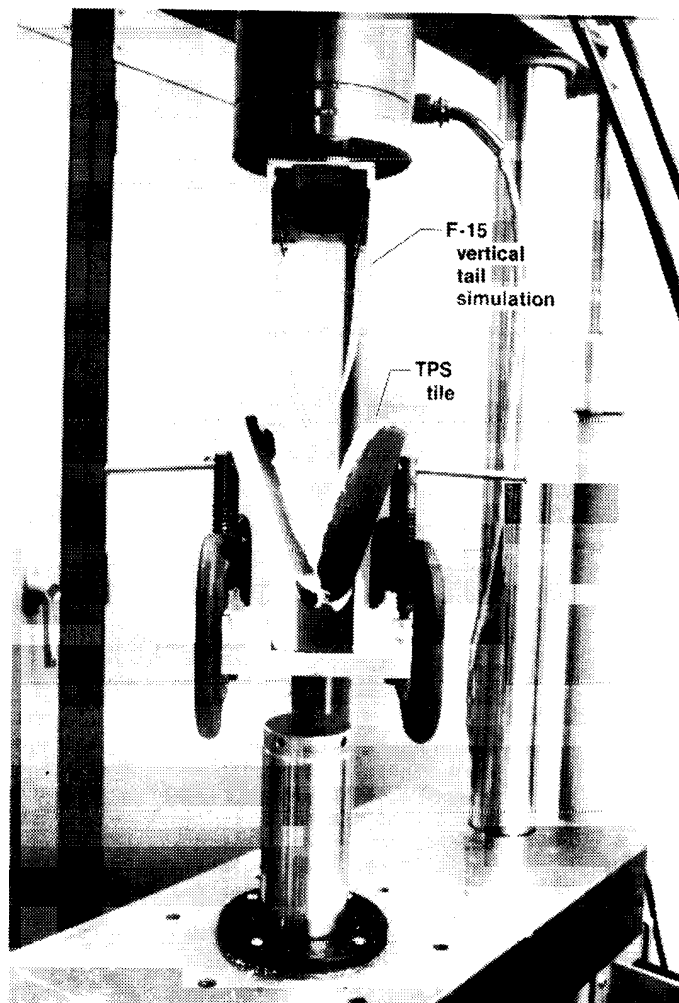
ECN 11321

Figure 12. Mode I fracture test.



ECN 11315

Figure 13. Mode 2 fracture test.



ECN 11317

Figure 14. Mode 3 fracture test.

